HYDRODYNAMIC IMPACT INSIDE A CYLINDRICAL CAVITY

YURIY N. SAVCHENKO[*], GEORGIY Y. SAVCHENKO[*] AND YURIY A. SEMENOV[♦]

[*]IHM (Institute of Hydromechanics of the National Academy of Sciences of Ukraine)
8/4 Zhelybova Street, Kiev, Ukraine
hydro.ua@gmail.com

[♦] University College London
Gower Street, London WC1E 6BT, UK
semenov@a-teleport.com

Abstract
Hydrodynamic loads acting on a cylindrical body moving inside a supercavity are investigated using both experimental and theoretical methods. Experimental studies of supercavitating models moving at speeds in the range from 400 *m/s* to 1000 *m/s* revealed a regime of bouncing motion, in which the rear part of an axisymmetric body periodically bounces against the free boundaries of the supercavity. The hydrodynamic force generated by the impacts and the behaviour of the cavity surface are of main concern in this paper. Analysis is performed in the approximation of two-dimensional potential flow of an ideal and incompressible liquid with negligible surface tension effects. The primary interest of the study is to investigate the effects of the cavity and body shapes on the added mass and the velocity distribution along the cavity surface immediately after an impact. The impulsive motion of an arc-shaped body inside a cylindrical cavity is studied based on the integral hodograph method, which makes it possible to derive analytic expressions for the flow potential and for the complex velocity in an auxiliary parameter plane and obtain a solution of the problem in parametric form. The problem is reduced to a system of two integro-differential equations in the unknowns velocity magnitude on the cavity surface and the angle between the velocity vector and the cavity boundary. These equations are solved numerically using the method of successive approximations. The obtained results revealed that the added mass of an arc impacting a cylindrical cavity depends heavily on its angle. As the angle tends to zero or the radius of the cavity tends to infinity, the obtained solution tends to that corresponding to a plate impacting a flat free surface.

1. Introduction

High-speed motion in water is known to be most efficient in the regime of developed cavitation. In the supercavitation regime, the formation of a developed cavity downstream of the cavitator is possible, this allowing the moving body to diminish or fully eliminate its contact with the water downstream of the cavitator. Because of this, there is little, if any, friction drag on the body surface covered by the cavity. In this case, the moving model experiences only hydrodynamic drag on the cavitator [1, 2, 3].

The motion of a high-speed supercavitating vehicle (HSSV) is instable in nature because of a torque produced by the hydrodynamic drag acting on the cavitator and the inertia force acting on the body further downstream. Besides, no buoyancy force acts on the vehicle inside the supercavity, and its weight is compensated by the hydrodynamic forces. This type of motion faces some challenges to control the stability of the motion. Experimental studies of supercavitating models moving at speeds in the range from 400 *m/s* to 1000 *m/s*, carried out at IHM, revealed a regime of bouncing motion, in which the rear part of an axisymmetric model periodically bounces against the boundaries of the supercavity. The interaction between the model and the cavity boundaries in bouncing motion is similar to water impacts. It is shown that the impact loads can lead to loss of the stability of the supercavitation motion and the structural stability of the model [4, 5, 6].

As known from ship hydrodynamics [7, 8], planing takes place if the Froude number exceeds a certain critical value

$$Fr = \frac{V}{\sqrt{g\sqrt[3]{Q}}} > 3,$$

where V is the speed, g is the gravitational acceleration, and Q is the water displacement. In this case, the hydrodynamic lift accounts for more than 95%, while the contribution of the hydrostatic lift diminishes to 4%.

As the speed increases, planning inevitably changes to bouncing planing ($Fr \gg 3$), in which the hull–liquid interaction is of impact character. The bouncing motion of suparcavitating objects inside the supercavity differs essentially from the motion of planing boats over a water surface. HSSVs execute periodic oscillations about the center of gravity, in which the stern bounces between the surrounding supercavity walls. Impacts with the walls at a speed of about 1,000 m/s may result in loss of stability and destroy the vehicle [5]. With a further velocity increase up to 1500 m/s, the density of saturated vapour inside the supercavity $\rho = 0.02$ kg/m^3 at the temperature, t $\approx 22^{\mathbf{o}}$C, becomes sufficient to produce an aerodynamic head pressure of 0.0225 MPa to support the HSSV without any contact with the water [7]

1.1 Experimental studies of supercavitating objects.

The bouncing motion of models was found out in the stability study of the inertial supercavitating motion of axisymmetric objects conducted as part of the program of experimental investigations at the Institute of Hydromechanics of the National Academy of Sciences of Ukraine [2, 4, 5, 9]. A schematic of the experimental setup equipped with a photorecording and speed measurement system is shown in Fig. 1.
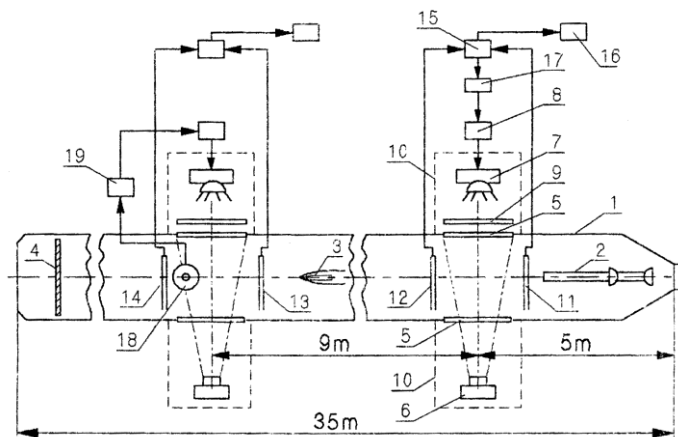
Figure 1. Launching tank schematic.

An electrochemical catapult 2 is installed at the head of a launching tank 1 of length 35 m. The catapult decomposes water into hydrogen and oxygen and uses the energy released in the burning of their mixture for launching models at speeds up to 1,550 m/s. At the end of the launching tank, models were caught with a catcher 4. The supercavitating flow pattern was recorded through twin glass windows 5 by photo TV cameras 6 using a pulse lighting system 7, 8, 9 with an exposure time from 2×10^{-6} s. The model speed was measured with contact sensors 11 - 14, inertia sensors 18, pulse shapers 15, and speed recorders 16.

The experiments were made with models of length, L, from 83 mm to 150 mm and diameter, D, from 7 mm to 10 mm with a cavitator diameter, d_n, from 1 mm to 1.5 mm. The model speed was from 880 m/s to 903 m/s.
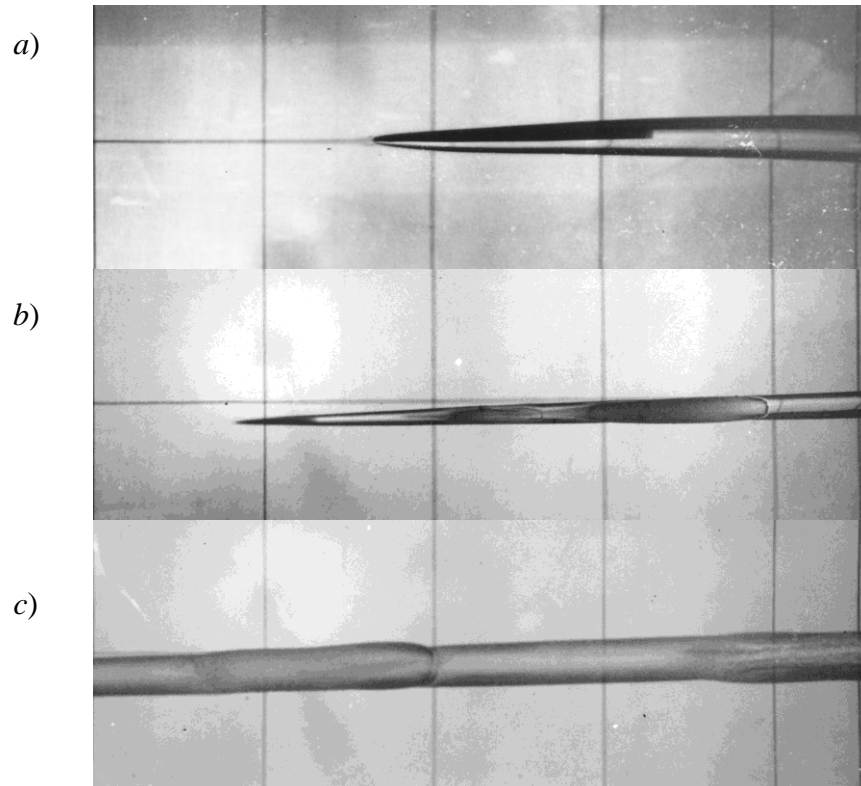
Figure 2. *a*) Supercavitating model in the supercavity at the instant of a bounce against the upper boundary of the cavity: $V = 910$ m/s, exposure time 2×10^{-6} s, $L = 150$ mm; $D = 10$ mm, $d_n = 1.2$ mm; *b*) a supercavitating model and a supercavity with bouncing marks: $L = 85$ mm, $D = 7.7$ mm, $d_n = 0.97$ mm, $V = 980$ m/s; *c*) supercavity with bouncing marks on the side walls: $L = 150$ mm, $D = 10$ mm, $d_n = 1.2$ mm, $V = 900$ m/s.
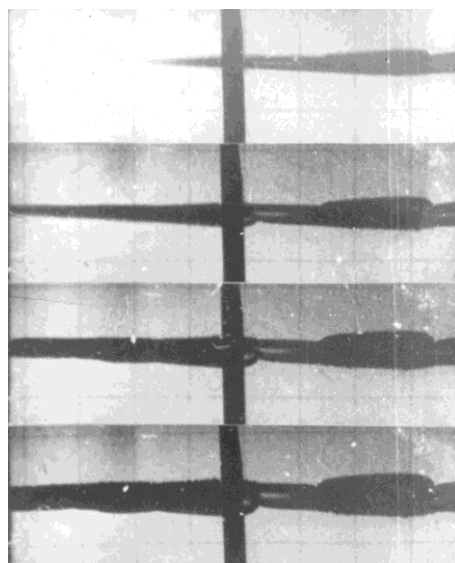
Figure 3. High-speed photos of the motion of a supercavitating model $V = 890$ m/s, $\Delta t = 2.4 \times 10^{-4}$ s, $L = 150$ mm, $D = 10$ mm, $d_n = 1.2$ mm.

Figures 2 and 3 show supercavities with marks of model bounces against the walls. The photos were taken using a high-speed X-Stream XS-4 video camera and pulse lighting with a pulse width of 2×10^{-6} *s*. As can be seem from Figs. 2 and 3, the marks of model bounces on the supercavity walls are 0.2 to 0.3 *m* apart, which at a model speed of 900 *m/s* sets up periodic bouncing with a frequency of about 1.5 *kHz*. In the assumption of harmonic oscillations $y = A\mathrm{Sin}\,\omega t$ of amplitude $A = 0.5D \approx 5\,mm$, the g-load on the stern of the model will be

$$\ddot{y} = A(2\pi n)^2 = 0.005(2\pi 1500)^2 \approx 45 \cdot 10^3 \cdot g \tag{1}$$

This g-load is comparable with that on a shell in a gun barrel and may deform models, which was occasionally observed in the experiments.

The following conclusions may be drawn from the analysis of the experimental data:
1. An indispensable condition for bouncing planing is a clearance between the model body and the supercavity boundary, $h > 0.15\ D$.
2. A model executed oscillations in the supercavity both in the vertical (Fig. 3) and in the horizontal (Fig. 2) plane passing through the supercavity axis. The position of the oscillation plane seems to depend on the location of the initial disturbance during the exit from the barrel.
3. The bouncing oscillations of a model in the supercavity are affected by the disturbances of the supercavity boundary caused by the cavitator oscillations in antiphase with the stern oscillations. They come to the stern with delay Δt

$$\Delta t = \frac{L}{V}, \tag{2}$$

where *L* is the model length and *V* is the model speed.
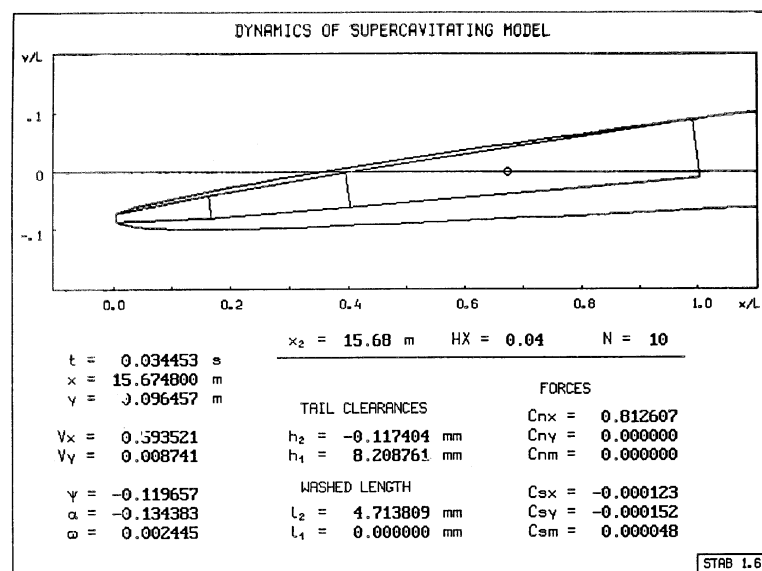
Figure 4. Simulation of the dynamics of a supercavitating model. Instant of a bounce against the upper boundary of the supercavity.

Fig. 4 shows a screenshot taken during the simulation of model oscillations in the supercavity, The mathematical model of supercavity shape calculation was based on the principle of independent cavity section evolution [1]. The simulation accounted for the model and cavity shape, the moment of inertia of the model, the position of the center of gravity, and the hydrodynamic forces on the cavitator and the stern of the model. If the delay Δt with which the

disturbances from the cavitator come to the model stern is half the bouncing period, the radial displacement of the cavity will be in phase with that of the stern, thus causing a resonance.

In view of (2), the resonance condition is

$$\frac{L}{V} = \frac{T}{2} = \frac{1}{2n}.$$ (3)

Hence it follows that the resonance frequency n_p is

$$n_p = \frac{V}{2L}.$$ (4)

At $L = 0.150$ *m* and $V = 900$ *m/s*, the resonance frequency is $n_p = 3$ *kHz*, which is 2 –3 times higher than the frequencies of steady-state bouncing observed in the experiments. The simulation has shown that for frequencies $n < n_p$ the cavity oscillations will have a stabilizing effect on the model oscillations in the cavity.

Depending on the model and cavity shape, the interaction of the model stern with the cavity boundary at their contact may be of penetration or impact character. In the case where the stern of a cylindrical body enters the water at an angle of attack and the area of contact with the water increases as the stern submerges, the interaction is of penetration character. Problems of this type are considered in [10 - 16]. In the case where the diameters of the body and the cavity are close and the shape of the boundaries is congruent over a considerable area, the interaction is of impact character, and the forces produced on impact are far greater than those in the case of penetration. This problem is considered in the next section.

2. Impulse solution for a circular arc impacting the free surface of the cylindrical cavity

The pioneering works on water impact problems are based on von Karman [10] impulse solution for a flat plate impacting the flat free surface of the half-space of the liquid. This solution is widely used as a model of various water impact problems of shaped bodies for which the actual shape is replaced by the equivalent plate. The von Karman solution implies that the free surface remained flat during impact, and the length of the equivalent plate equals to the length between intersection points of the actual body and the free surface. Further development of the water impact models has been done by Wagner [11] who introduced the correction of the length of the equivalent plate taking into account the free surface rise due to the liquid displacement by the body. After Wagner's correction the length of the plate included the effect of the local free surface elevation, and therefore the length itself was the part the solution.

Most of studies on water impact problems arising in various marine applications deal with a flat free surface. In the present paper we study the effects of the free surface shape on the impulse forces generated by the impacts between the HSSV vehicles and the free surface of the cylindrical supercavity.

We consider an arc of circle of the radius R and angle 2φ which impacts the free surface at time $t = 0$. Immediately after the impact at time $t = 0^+$, the velocity of the circular arc is V directed downward as shown in figure 5a. The liquid is assumed to be ideal and incompressible, and the flow is irrotational. The gravity and surface tension effects are ignored. Based on the dynamic equivalence, the body entry speed can be regarded zero and the flow comes from $y = -\infty$ with velocity V. We define a Cartesian system xy with its origin at the bottom of the arc.
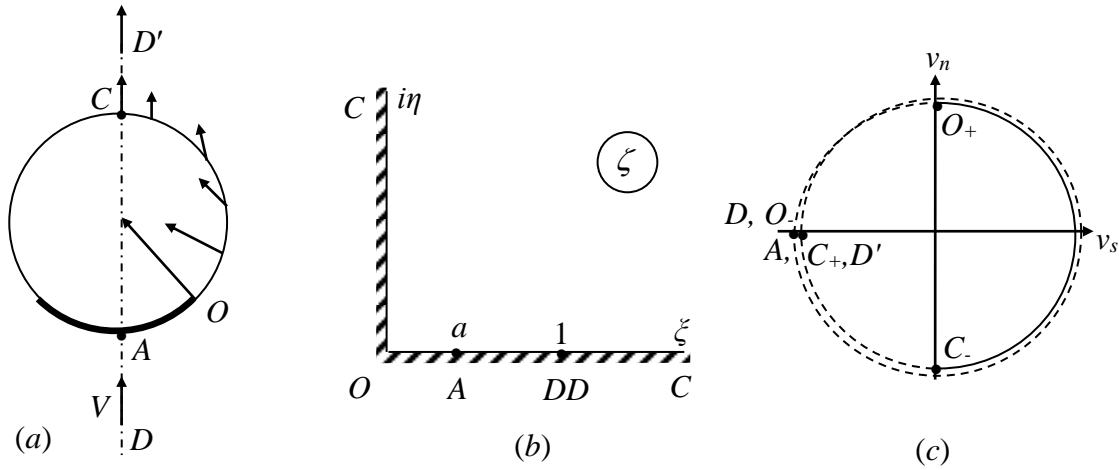
Figure 5. (a) sketch of the impulse impact of the circular arc onto the cylindrical free surface; (b) ζ – pane; (c) variation of the function $\omega = \tan^{-1}(v_n / v_s)$ along the whole boundary of the fluid region. The continuous and step changes in ω are shown by solid and dashed lines, respectively.

The problem is to determine the function $w(z)$ which conformally maps the physical plane z onto the complex-velocity potential region w. We shall use the integral hodograph method [16]. In the method a parameter plane ζ is introduced. Instead of finding $w(z)$ directly, two complex functions, dw/dz, which is the complex velocity, and the function $dw/d\zeta$ both are sought in the ζ – plane in the integral form. Once these two functions are found, the relation between the parameter and stationary planes can be determined as follows:

$$z(\zeta) = z_O + \int_0^\zeta \frac{dz}{d\zeta} d\zeta = z_O + \int_0^\zeta \frac{dw}{d\zeta} \bigg/ \frac{dw}{dz} d\zeta \,, \tag{5}$$

where z_O is the position of point O.

Based on the method of Chaplygin (see §5 of Chapter 1 in Gurevich (1965)) we choose the first quadrant of the ζ – plane shown in figure 1*b* as the parameter region which corresponds to the flow region of $x \geq 0$ in the physical plane in figure 5*a*. The functions dw/dz and $dw/d\zeta$ conformally map the parameter region onto the regions of the complex velocity and the derivative of the complex potential. Based on the theorem of conformal mapping three points in the parameter plane can be chosen arbitrary, which are taken as O (intersection point of the body surface and the free surface), D (a point at infinity) and A (stagnation point at the bottom of the arc), as shown in figure 5*b*. The imaginary axis corresponds to the free surface OC. The interval $0 \leq \xi \leq a$ of the real axis corresponds to the circular arc, and the interval $a \leq \xi \leq 1$ corresponds to the symmetry line AD. The rest of the positive real axis ($1 < \xi < \infty$) corresponds to the symmetry line CD'. In order to determine the functions dw/dz and $dw/d\zeta$ we shall formulate appropriate boundary-value problems for each of these functions in the ζ – plane.

At this stage it is assumed that the velocity modulus along the free surface, that is along the positive part of the imaginary axis,

$$\left|\frac{dw}{dz}\right| = v(\eta), \quad 0 < \eta < \infty, \; \xi = 0. \tag{6}$$

is known. This function will be determined below in the following. In the frame of reference attached to the flat plate, the normal velocity component equals zero due to the impermeability condition. This means that the argument χ of the complex velocity along the interval $0 \leq \xi \leq a$ of the real axis equals $-\beta(\xi)$, where $\beta(\xi)$ is the slope of the arc as function of the variable ξ. By using these notations we can write the function $\chi(\xi)$ as follows

$$\chi(\xi) = \arg\left(\frac{dw}{dz}\right) = \begin{cases} -\beta(\xi), & 0 < \xi < a, \quad \eta = 0, \\ -\pi/2, & a < \xi < \infty, \quad \eta = 0. \end{cases} \tag{7}$$

The problem is then to find a function dw/dz in the first quadrant of the parameter plane which satisfies the given boundary conditions. The formula

$$\frac{dw}{dz} = v_\infty \exp\left[\frac{1}{\pi}\int_0^\infty \frac{d\chi}{d\xi}\ln\left(\frac{\varsigma+\xi}{\varsigma-\xi}\right)d\xi - \frac{i}{\pi}\int_0^\infty \frac{d\ln v}{d\eta}\ln\left(\frac{\varsigma-i\eta}{\varsigma+i\eta}\right)d\eta\right] \tag{8}$$

provides a solution of the mixed boundary-value problem (6) - (7) in the first quadrant of the complex $\varsigma-$plane. Here, $v_\infty = v(\eta)_{\eta\to\infty}$ is the velocity magnitude at point C. The argument of the complex velocity undergoes a step change at the point $\varsigma = a$ corresponding to the corner at point A in the physical plane, $\beta(a) = 0$. Substituting equation (7) into the first integral in (8) we finally obtain an expression for the complex velocity in the ς -plane as

$$\frac{dw}{dz} = v_\infty\left(\frac{a-\varsigma}{a+\varsigma}\right)^{\frac{1}{2}}\exp\left[\frac{1}{\pi}\int_0^a \frac{d\beta}{d\xi}\ln\left(\frac{\xi-\varsigma}{\xi+\varsigma}\right)d\xi - \frac{i}{\pi}\int_0^\infty \frac{d\ln v}{d\eta}\ln\left(\frac{\varsigma-i\eta}{\varsigma+i\eta}\right)d\eta - i\beta_0\right], \tag{9}$$

where $v_\infty = v(\eta)_{\eta\to\infty}$. It is seen that the complex velocity function has only one zero of order $1/2$ at point $\varsigma = a$.

In order to analyse the behaviour of the velocity potential along the free surface, it is useful to introduce the unit vectors $\boldsymbol{n}$ and $\boldsymbol{\tau}$ which are normal and tangent to the free surface, respectively. The normal vector is directed outward from the fluid region while the spatial coordinate along the free surface s increases along the free surface with the fluid region taken on the left (figure 5). With this notation,

$$dw = (v_n + v_s)ds, \tag{10}$$

where v_n and v_s are the tangential and normal velocity components, respectively. Let θ denote the angle between the velocity vector on the free surface and the unit vector $\boldsymbol{\tau}$, $\theta = \tan^{-1}(v_n/v_s)$; its behaviour along the boundary of the fluid region is shown in figure 2.

The argument of the derivative of the complex potential, $\vartheta(\varsigma) = \arg(dw/d\varsigma)$, can be determined on the whole boundary of the flow domain as follows

$$\vartheta(\varsigma, t) = \arg\left(\frac{dw}{d\varsigma}\right) = \begin{cases} 0, & 0 < \xi < \infty, \quad \eta = 0, \\ \arg\left(\frac{dw}{ds}\right) - \pi/2, & \xi = 0, \quad 0 < \eta < \infty \end{cases} \tag{11}$$

By introducing the continuous function $\lambda(\eta, t)$

$$\omega(\zeta) = \arg\left(\frac{dw}{ds}\right) = \begin{cases} \pi, & 1 < \xi < \infty, \quad \eta = 0, \\ -\pi, & 0 < \xi < 1, \quad \eta = 0, \\ \lambda(\eta), & 0 < \eta < \infty, \quad \xi = 0. \end{cases} \qquad (12)$$

The function $\lambda(\eta)$ increases from $\lambda(0) = -\pi/2$ at point O to $\lambda_{\infty} = \lambda(\eta)_{\eta\to\infty} = \pi/2$ at point C.

The derivative of the potential can be written in the following integral formula (Semenov & Iafrati 2006):

$$\frac{dw}{d\varsigma} = K(t)\exp\left[-\frac{1}{\pi}\int_0^{\infty}\frac{d\vartheta}{d\xi'}\ln\left(\varsigma^2 - \xi'^2\right)d\xi' + \frac{1}{\pi}\int_0^{\infty}\frac{d\vartheta}{d\eta'}\ln\left(\varsigma^2 + \eta'^2\right)d\eta' + i\vartheta(\infty)\right], \qquad (13)$$

where K is a real factor and $\vartheta_{\infty} = \vartheta(\zeta)_{|\varsigma|\to\infty}$. By substituting (11) and (12) into (13) and evaluating the integrals over each step change of the function $\vartheta(\zeta)$ at point D ($\zeta = 1$), we obtain

$$\frac{dw}{d\zeta} = K\frac{1}{\left(\zeta^2 - 1\right)^2}\exp\left[\frac{1}{\pi}\int_0^{\infty}\frac{d\theta}{d\eta}\ln\left(\zeta^2 + \eta^2\right)d\eta\right], \qquad (14)$$

where $\theta(\eta) = \omega(\zeta)_{\zeta=i\eta}$.

The equations (9) and (14) include two unknown parameters K, a and v_{∞} which are determined from the following physical considerations. The velocity magnitude at point D ($\zeta = 1$) is chosen as the reference velocity, therefore it is equal to 1,

$$v_{\infty}\left|\frac{1-a}{1+a}\right|\exp\left[\frac{1}{\pi}\int_0^a\frac{d\beta}{d\xi}\ln\left|\frac{\xi-1}{\xi+1}\right|d\xi - \frac{2}{\pi}\int_0^{\infty}\frac{d\ln v}{d\eta}\arctan\eta d\eta\right] = 1. \qquad (15)$$

The length of the circular arc is

$$\int_0^a\frac{ds}{d\xi}d\xi = R\varphi, \qquad (16)$$

$$\frac{ds}{d\xi} = \left|\frac{dz}{d\varsigma}\right|_{\varsigma=\xi} = \left|\frac{dw}{d\varsigma}\middle/\frac{dw}{dz}\right|_{\varsigma=\xi} = \frac{K}{v_{\infty}}\frac{1}{(\xi^2-1)^2}\left|\frac{\xi+a}{\xi-a}\right|^{\frac{1}{2}}$$

$$\times\exp\left[\frac{1}{\pi}\int_0^{\infty}\frac{d\theta}{d\eta}\ln(\eta^2 + \xi^2)d\eta - \frac{1}{\pi}\int_0^a\frac{d\beta}{d\xi'}\ln(\xi'^2 - \xi^2)d\xi' + \frac{1}{\pi}\int_0^{\infty}\frac{d\ln v}{d\eta}2\tan^{-1}\left(\frac{\eta}{\xi}\right)d\eta\right] \qquad (17)$$

The mass balance between the incoming liquid and that coming into the cavity

$$\int_0^{R(\pi-\varphi)}v_n ds = R\sin\varphi, \qquad \text{or} \qquad \int_0^{\infty}v\sin\theta\frac{ds}{d\eta}d\eta = \sin\varphi, \qquad (18)$$

where $v_n = v\sin\theta$ and $v(\eta) = v_{\infty}\exp\left(-\int_{\eta}^{\infty}\frac{d\ln v}{d\eta'}d\eta'\right)$.

Equations (9) and (14) contain the functions $\beta(\xi)$, $v(\eta)$ and $\lambda(\eta)$, which have to be determined from the kinematic boundary condition on the free surface and the wetted surface of the body.

Body surface boundary condition: integro-differential equation for function $\beta(\xi)$.

By integrating (17) along the real axis of the parameter region, we can determine the spatial coordinate along the body as a function of the parameter variable ξ

$$s(\xi) = \int_0^{\xi} \frac{ds}{d\xi'} d\xi'. \tag{19}$$

Since the function $\beta = \beta(s)$ is known on the wetted body surface OA corresponding to the interval $0 \le \xi \le a$, the function $\beta = \beta(\xi)$ is determined from the following equation:

$$\frac{d\beta}{d\xi} = \frac{d\beta}{ds} \frac{ds}{d\xi}. \tag{18}$$

By using $ds / d\xi$ from (15), this equation takes the form

$$\frac{d\beta}{d\xi} = \frac{K}{v_{\infty}} \kappa[s(\xi)] \frac{1}{(\xi^2-1)^2} \left| \frac{\xi+a}{\xi-a} \right|^{\frac{1}{2}}$$
$$\times \exp\left[\frac{1}{\pi} \int_0^{\infty} \frac{d\lambda}{d\eta} \ln(\eta^2+\xi^2) d\eta - \frac{1}{\pi} \int_0^a \frac{d\beta}{d\xi'} \ln(\xi'^2-\xi^2) d\xi' + \frac{1}{\pi} \int_0^{\infty} \frac{d\ln v}{d\eta} 2\tan^{-1}\left(\frac{\eta}{\xi} \right) d\eta \right], \tag{19}$$

where $\kappa(s) = d\beta / ds = 1/R$ is the curvature of the circle arc.

Kinematic boundary condition on the cavity surface: integral equation for the function $d\ln v / d\eta$.

During the impulse impact the free surface does not change. The slope of the free surface can be obtained using the relation, $dz / d\zeta = (dw / d\zeta) / (dw / dz)$, and equations (9) and (14)

$$\delta(\eta) = \arg\left(\frac{dz}{d\zeta} \bigg|_{\zeta=i\eta} \right) = \arg\left(\frac{dw}{d\zeta} \bigg|_{\zeta=i\eta} \right) - \arg\left(\frac{dw}{dz} \bigg|_{\zeta=i\eta} \right) = \theta(\eta) - \arg\left(\frac{dw}{dz} \bigg|_{\zeta=i\eta} \right). \tag{20}$$

Taking the argument of the complex velocity from (9) at $\zeta = i\eta$ and substituting the result into (20) we obtain the following integral equation respect the function $d\ln/d\eta$

$$\frac{1}{\pi} \int_0^{\infty} \frac{d\ln v}{d\eta'} \ln\left| \frac{\eta'-\eta}{\eta'+\eta} \right| d\eta' + \frac{2}{\pi} \int_0^{\infty} \frac{d\beta}{d\xi} \tan^{-1}\frac{\eta}{\xi} d\xi - \tan^{-1}\frac{\eta}{a} = \delta(\eta) - \theta(\eta), \tag{21}$$

where $\theta(\eta)$ is the velocity angle to the cavity surface is determined from the following condition. The velocity generated on the cavity surface during the impulse impact should has its direction which is perpendicular to the free surface. This fact follows from Euler equations in cases of constant pressure along the free surface. Therefore, the tangential component of the velocity remains constant during the impact, $v\cos\theta = \sin\delta$, from which the function $\theta(\eta)$ can be determined

$$\theta = \cos^{-1}\left(\frac{\sin\delta}{v} \right). \tag{22}$$

The impulse force P generating the flow which potential is ϕ can be evaluated using Cauchy - Lagrange integral

$$P = -\rho \int_{-L}^{L} \phi(s) ds = m\rho L^2 V, \tag{23}$$

where m is the coefficient of the added mass of the circular arc, and $L = R\sin\varphi$ is the projection onto the $x-$axis.

Results and discussion

The solution procedure of the system of integral equations (19) and (21) is based on the method of successive approximations. In discrete form, the solution is sought on a fixed set of points ξ_j, $j = 1,...,M$ distributed along the real axis of the parameter region and on a fixed set of points η_j, $j = 1,...,N$ distributed along the imaginary axis as geometric series. In the most calculations below, $N = 400$ and $M = 200$. The smallest intervals near the edge of the arc (point O) was chosen $\Delta\eta_1 = \eta_1 - \eta_0 = \xi_1 - \xi_0 = 10^{-5}$. Equation (19) converges rapidly requiring few iterations, while equation (21) together with (22) take several hundred iterations to reach the tolerance $\varepsilon = 10^{-5}$.

a)   b)

c)   d)
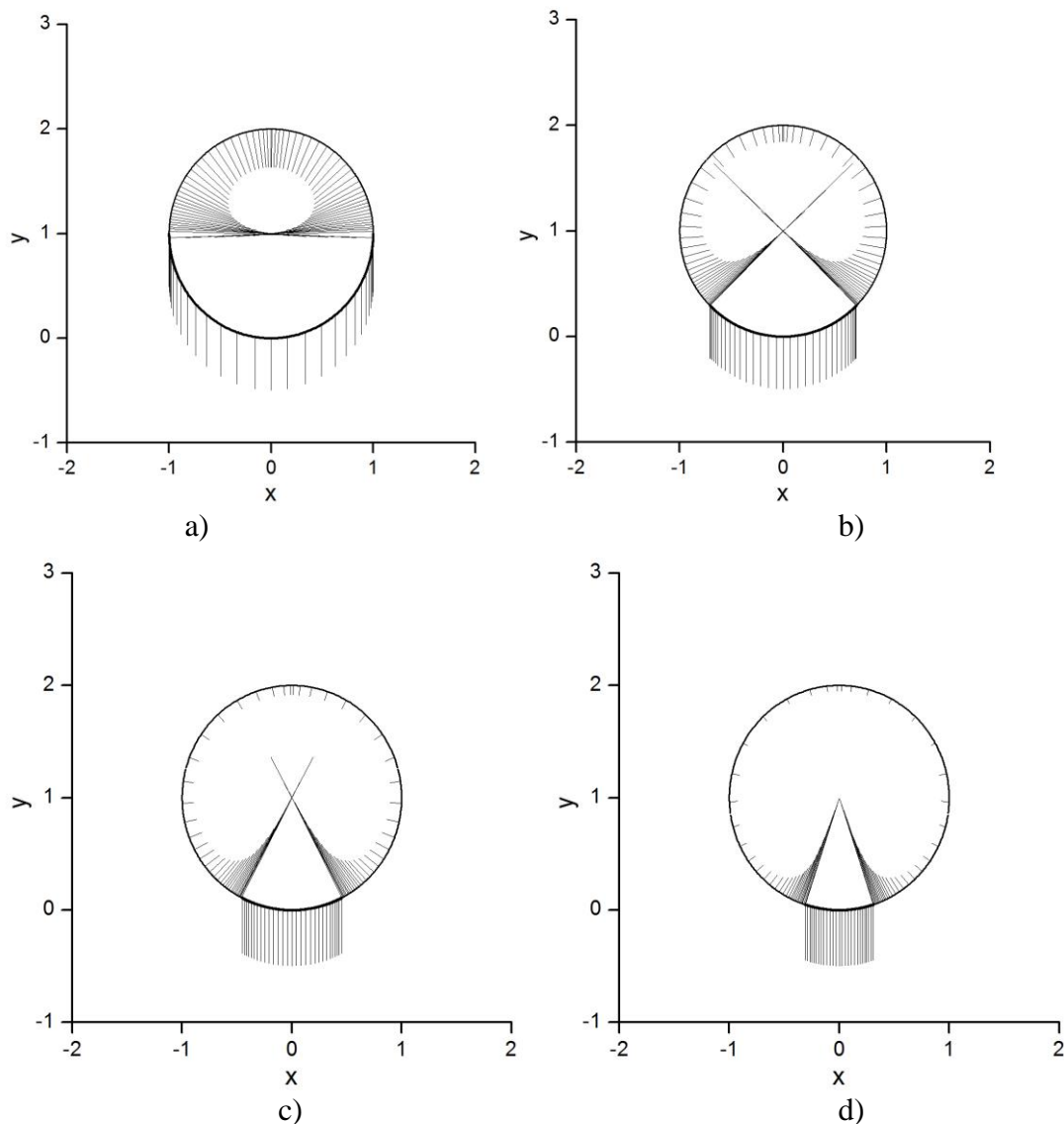
Figure 6. Velocity distribution along the cylindrical cavity for different angles of the arc: a) $\varphi = 0.5\pi$; b) $\varphi = 0.25\pi$; c) $\varphi = 0.15\pi$ and c) $\varphi = 0.1\pi$.

Velocity distributions along the cylindrical cavity are shown in figure 6 for different angles of the circular arc. The results are shown in the system of coordinates related to the calm liquid at infinity. The thick lines correspond to the arc and velocity vectors are shown by the thin lines

perpendicular to the cylindrical cavity shape (inside the circle) and to the circular arc (outside the circle). At the edge of the arc the velocity magnitude tends to infinity (these lines were shortened), and gradually decrease away from the arc. As the length of the arc increases, the minimal velocity at the top of the cavity also increases. It is caused by the larger amount of the liquid which the arc push inside the cavity. As the angle of the arc becomes smaller and smaller the cavity surface flattener near the arc and the solution gradually tends to that corresponding to the plate impacting the flat free surface.
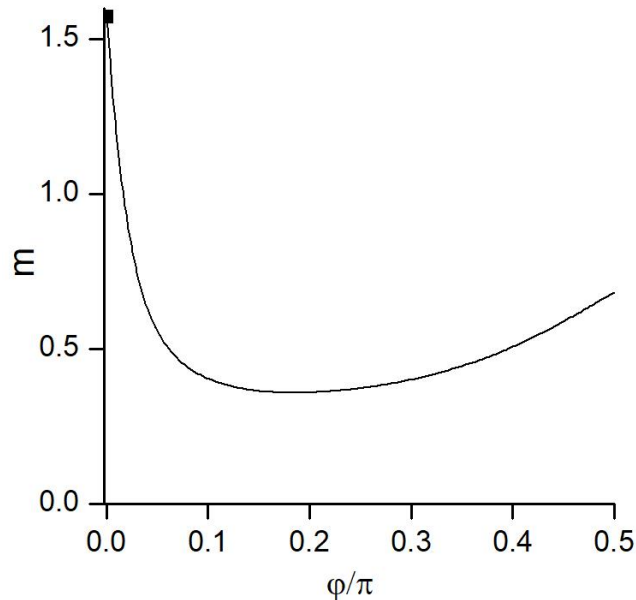
Figure 7. Coefficient of the added mass for the circular arc impacting the cylindrical cavity vs angle of the arc. At φ=0 (solid square) the circular arc becomes the flat plate for which $m = \pi/2$.

The coefficient of the added mass versus the arc angle is shown in figure 7. For very small angle φ, the value of the coefficient tends to $\pi/2$ that corresponds to the plate impacting the free surface. However, it rapidly decreases for relatively moderate values $0 < \varphi/\pi < 0.1$. Such behaviour of the added mass could be explained as the effect of the shape of the body which reduce the liquid acceleration near the arc. Similar effect was observed in the paper [15], who studied the water entry problem of the circular arc based on the Wagner's approach. For the angle $0.2 < \varphi/\pi < 0.5$ the coefficient of the added mass increases. This may occur due to choice of the length $L = R\sin\varphi$ in (23). Indeed, the length L is slowly increases as $\varphi/\pi \to 0.5$, while the area of liquid displaced by the arc increases proportionally to the length $R\varphi$.

Conclusions.
The sudden vertical motion of the circular arc impacting the wall of the cylindrical cavity has been investigated. The fully nonlinear hydrodynamic problem has been solved through the derivation of the flow potential which has been obtained applying the integral hodograph method. The problem is reduced to a system of integral and integro-differential equations in terms of the slope of the body and velocity magnitude along the free surface after the kinematic boundary conditions on the body and free surface are imposed. The numerical results are presented over a wide range of the arc angles $0 < \varphi/\pi < 0.5$ in terms of the velocity distribution along the free surface. The non monotonic behaviour of the added mass coefficient, m, for different arc angles is revealed. For very small angles of the arc, φ, the coefficient of the added mass tends to $\pi/2$ that corresponds to the added mass coefficient of the flat plat impacting the flat free surface. However, small change of the angle φ causes the significant decrease of m to

the value about $m = 0.5$. The present study makes the possibility to evaluate impulse forces acting on the vehicles moving at high speeds inside the supercavity, that is necessary to predict overall dynamics of high-speed supercavitating vehicles.

In actual practice, the following should be taken into account: the supercavity is filled with saturated water vapor, whose density is lower than the air density by a factor of several tens; the water vapor flows about the model body at a supersonic velocity with a Mach number of about 3; the supercavity boundary is not smooth and has a spray structure typical of high-velocity jet flows. However, these neglected factors reduce dynamic loads. So the estimation of the hydrodynamic forces by the above-described kinematic model will give maximum possible values, which may be used in assessing the required HSSV strength and motion stability. It should be noted that the body of a supercavitating HSSV interacts with the supercavity boundaries that it forms itself using its cavitator. This factor should be used to form a cavity boundary with properties and a shape that offer reduced impact loads.

References

1. Logvinovich, G. 1972 *Hydrodynamics of free-boundary flows*. US Dept. Commerce, Washington, DC, USA, translated from the Russian (NASA-TT-F-658).
2. Savchenko Yu.N., Vlasenko Yu.D., Semenenko V.N. 1998 Experimental study of high-speed cavitation flows. *Hydromechanics*. **72**, 103 - 111 (in Russian)
3. Savchenko, Yu. N. 1997 Investigation of High-Speed Supercavitating Underwater motion of bodies. *AGARD workshop report R-827*, Kiev, 1-3 September.
4. Savchenko, Y. N. 2001 Control of supercavitation flow and stability of supercavitating motion. Lecture notes for the RTO AVT/VKI special course on supercavitating flows, von Karman Institute for Fluid Dynamics, Rhode Saint Genèse, Belgium, 12 - 16 February.
5. Savchenko, Yu.N., Semenenko, V.N., and Putilin, S.I. 2000 Unsteady supercavitated motion of bodies. *Int. J. of Fluid Mechanics Research*. **27** (1), 109 – 137.
6. Semenenko, V. N. 2001 Artificial Supercavitation: Physics and Calculation. Lecture Notes for the RTO AVT/VKI Special Course on Supercavitating Flows, von Karman Institute for Fluid Dynamics, Rhode Saint Genèse, Belgium, 12 - 16 February.
7. Voytkunsky, Y. I., Pershitz R. Y. & Titov I. A. 1960 *A guide to the theory of the ship*. SudpromGIZ (in Russian).
8. Faltinsen, O. M. 2005 *Hydrodynamics of High-speed Marine Vehicles*. Cambridge University Press.
9. Vlasenko Yu.D. 1998 Experimental investigations of high-speed unsteady supercavitating flows. *Third International Symp. on Cavitation*, **2**, 39 - 44, Grenoble.
10. von Karman, T. 1929 The impact of seaplane floats during landing. *NACA Tech. Note 321*. Washington, DC.
11. Wagner, H. 1932 Über Stoßund Gleitvorgänge an der Oberfläche von Flüssigkeiten. *Z. Angew. Math. Mech*. **12**, 192 – 215.
12. Savchenko G.Y. & Савченко Y.N. 2013 Gliding cylinder in supercavity. //*Applied Hydromechanics*. **15** (3), 79 – 84.
13. Paryshev, E.V. 2006 Approximate Mathematical Models in High-Speed Hydrodynamics. *Journal of Engineering Mathematics*, **55**, 41 - 64.
14. Kirschner, I.N. & Arzoumanian, S. H. 2008 Implementation and extension of Paryshev's model of cavity dynamics. International conference on innovative approaches to further increase speed of fast marine vehicles, moving above, under and in water surface. *SuperFAST'2008*, July 2-4, 2008, Saint-Petersburg.
15. Vasin, A.D. & Paryshev, E. V. 2001 Immersion of a cylinder in a fluid through a cylindrical free surface. *Fluid Dynamics*, **36** (2), 169 – 177.
16. Semenov, Y. A. & Iafrati, A. 2006 On the nonlinear water entry problem of asymmetric wedges. *J. Fluid Mech*. **547**, 231–256.